A Hybrid Battery Model for Prognostics in Small-size Electric UAVs

Gina Sierra[1], Marcos Orchard[2], Chetan Kulkarni[3], and Kai Goebel [4]

[1,2] *Department of Electrical Engineering, University of Chile, Santiago 8370448, Chile*
gina.sierra@ing.uchile.cl
morchard@ing.uchile.cl

[3] *SGT Inc., NASA Ames Research Center, Moffett Field, CA 94035, USA*
chetan.s.kulkarni@nasa.gov

[4] *NASA Ames Research Center, Moffett Field, CA 94035, USA*
kai.goebel@nasa.gov

ABSTRACT

Electric Unmanned Aerial Vehicles (UAVs) experience problems and risks associated with battery aging and abuse effects. Therefore, a Battery Health Management (BHM) system is necessary to make the battery a safe, reliable, and cost-efficient solution. BHM systems are essential to ensure that the mission goal(s) can be achieved and to aid in online decision-making activities such as fault mitigation and mission replanning. To accomplish these tasks, we have adopted a model-based prognostics architecture for battery-powered UAVs where a battery model is used as the basis of two sequential task, (*i*) the State of Charge (SOC) estimation, and (*ii*) the End of Discharge (EOD) prediction. Small-size aircraft usually have weight, size and cost constraints. Therefore, there is a need to accurately (i) estimate the SOC, and (ii) predict the EOD time of Li-Po batteries in small-size UAVs that can operate in constrained environments. This work proposes a modification to an electrochemistry-based battery model that allows reducing computational resources without losing accuracy in prognostic results. The resulting hybrid battery model is validated and applied to prognostic of the EOD time in discharge cycles of a Li-Po battery of a small size quadcopter that performs delivery missions. Prediction results using the proposed hybrid battery model are shown to be very accurate while its estimation and prediction processing times are significantly lower than processing times using the electrochemistry-based battery model.

1. INTRODUCTION

In recent years, Unmanned Aerial Vehicles (UAVs) have become increasingly popular because they can perform complex missions without human intervention. By its wing type, UAVs can be categorised into the following types: fixed-wing, rotary-wing and flapping-wing. Multicopters, a type of rotary-wing aircraft with at least three independent rotors and propellers, have recently emerged as the preferred platform since they are mechanically simple, highly maneuverable and enable safe and low-cost experimentation and operation in three dimensions. Unlike their fixed-wing counterparts, they can also hover in place, and take off and land vertically, (Valavanis & Vachtsevanos, 2015).

Power required is strongly determined by the total weight of the aircraft. The greater the weight, the greater the power required by the craft. Consequently, flight endurance is shorter when aircraft are heavier. Lithium Polymer (Li-Po) batteries are commonly used in UAVs as the primary power source because of their high-density energy. However, battery-powered UAVs experience problems and risks associated with the use of batteries as the primary Energy Storage Devices (ESD), namely, aging effects and operational abuse. The battery capacity decreases over time and use. Factors such as the room temperature of storage and usage, the State of Charge (SOC) in which the battery is stored, the discharge rate, overcharges or over-discharges affect its capacity (Mikolajczak, Kahn, White, & Long, 2011). Also, battery performance is strongly determined by characteristics such as the current discharge rate, depth of discharge, or the internal temperature.

Therefore, Battery Health Management (BHM) systems have emerged to make the battery a safe, reliable, and cost-efficient solution. BHM systems are essential to verify if the mission goal(s) can be achieved and to aid in online decision-making

activities such as fault mitigation and mission replanning. To accomplish these tasks, State of Charge (SOC) estimation and End of Discharge (EOD) prognostic are fundamental. However, as in many other state estimation problems, the SOC is not observable; namely, it can not be directly measured, and it has to be inferred from indirect but statistically related measurements (e.g., battery voltage, discharge current, and temperature) (Pola et al., 2015).

BHM systems for battery-powered UAVs have adopted a model-based prognostics architecture (Daigle & Goebel, 2013) where the battery is being monitored, and one develops a battery model describing how the system evolves in time in response to its inputs (Daigle, 2016a). Usually, the current is considered as an input. That model is used as the basis of two sequential problems, (*i*) the SOC estimation problem, and (*ii*) the EOD prediction problem.

In (Saha, Quach, & Goebel, 2011, 2012; de Souza Candido, Kawakami Harrop Galvao, & Yoneyama, 2014) authors have carried out SOC estimation and EOD time prognosis based on Particle Filter (PF). In contrast, (Cuong et al., 2013; Bole, Daigle, & Gorospe, 2014; Hogge et al., 2015) used Unscented Kalman Filter (UKF) for the same purpose. Both methods gave satisfactory results; however, PF is emerging as the preferred method because it appears to exhibit somewhat better performance than UKF (Walker, Rayman, & White, 2015).

Battery models with different levels of granularity have been explored and evaluated regarding their performance for estimation and prognosis. The results showed that higher granularity and lower levels of abstraction typically give more accurate predictions (Saha et al., 2011). Consequently, models that provide high accuracy usually are complex and require a large number of parameters, which is problematic for real-time applications.

Besides that, small-size aircraft specifically have weight, size and cost constraints. Consequently, as small-size UAVs become more prevalent, the need for computationally efficient software will increase. The improvement of efficiency in mobile software for drones and mobile devices is arising as a new research topic as companies explore the use of drones for delivering and other complex tasks (Banerjee & Roychoudhury, 2017). Therefore, there is a emerging need to accurately (i) estimate the State of Charge (SOC), and (ii) predict the End of Discharge (EOD) time of Li-Po batteries in small-size multirotors that can operate in constrained environments.

In order to decrease computational resources in battery prognostic, this work proposes a slight modification to the electrochemistry-based battery model by (Daigle & Kulkarni, 2013) to reduce its complexity without losing accuracy. In particular, an empirical parameterization of the equilibrium potential is proposed instead of the electrochemistry characterization given in (Daigle & Kulkarni, 2013). Since the resulting model is a compound of electrochemistry and empirical characterizations, we consider the model herein as a hybrid model. Prognostics results using the hybrid model for a Li-Po battery of a small-size quadcopter that performs delivery missions are evaluated in terms of EOD expectations, the Just-In-Time Point value, and the $\alpha - \lambda$ metric. In addition, the estimation and prediction processing times when the hybrid model is used are measured in order to evaluate its efficiency concerning estimation and prediction processing times when the original electrochemistry-based battery model is used.

The paper is organized as follows. Section 2 describes the electrochemistry-based battery model and the proposed modifications to reduce its complexity. Also, model validation is provided in this Section. In Section 3, the hybrid model is used to perform SOC estimations and EOD predictions on discharge cycles of a Li-Po battery of a small-size quadcopter that performs delivery missions. In addition, results are presented and discussed. Section 4 concludes the paper.

2. HYBRID BATTERY MODEL

This section introduces the battery model by (Daigle & Kulkarni, 2013) which is derived from a simplified set of electrochemical equations governing charge flow and voltage drops at the cathode, anode, and separator layers of a Li-ion battery. Then, a modification to the characterization of the equilibrium potential is described. Finally, the identified model parameters are presented and a validation of the model for a variable loading is made.

In the model by (Daigle & Kulkarni, 2013), the voltage terms of the battery are expressed as functions of the amount of charge in the electrodes (the states of the model). Each electrode, positive (subscript p) and negative (subscript n), is split into two volumes, a surface layer (subscript s) and a bulk layer (subscript b). The differential equations for the battery describe how charge moves through these volumes. The charge (q) variables are described using:

$$\dot{q}_{s,p} = i_{app} + \dot{q}_{bs,p} \tag{1}$$

$$\dot{q}_{b,p} = -\dot{q}_{bs,p} + i_{app} - i_{app} \tag{2}$$

$$\dot{q}_{b,n} = -\dot{q}_{bs,n} + i_{app} - i_{app} \tag{3}$$

$$\dot{q}_{s,n} = -i_{app} + \dot{q}_{bs,n}, \tag{4}$$

where i_{app} is the applied electric current. The term $\dot{q}_{bs,i}$ describes diffusion from the bulk to surface layer for electrode i, where $i = n$ or $i = p$.

$$\dot{q}_{bs,i} = \frac{1}{D}(c_{b,i} - c_{s,i}) \tag{5}$$

where D is the diffusion constant. The c terms are lithium ion

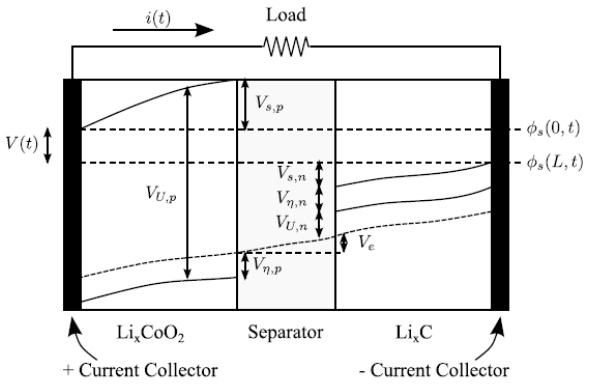

Figure 1. Battery voltages.

concentrations:

$$c_{b,i} = \frac{q_{b,i}}{v_{b,i}} \tag{6}$$

$$c_{s,i} = \frac{q_{s,i}}{v_{s,i}} \tag{7}$$

Here, $c_{v,i}$ is the concentration of charge in electrode i, and $v_{v,i}$ is the total volume of charge storage capability. It is defined $v_i = v_{b,i} + v_{s,i}$. Note now that the following relations hold:

$$q_p = q_{s,p} + q_{b,p} \tag{8}$$

$$q_n = q_{s,n} + q_{b,n} \tag{9}$$

$$q^{max} = q_{s,p} + q_{b,p} + q_{s,n} + q_{b,n} \tag{10}$$

It can also express mole fractions (x) based on the q variables:

$$x_i = \frac{q_i}{q^{max}}, \tag{11}$$

$$x_{s,i} = \frac{q_{s,i}}{q^{max}_{s,i}}, \tag{12}$$

where

$$q^{max}_{s,i} = q^{max}\frac{v_{s,i}}{v_i}, \tag{13}$$

and $q^{max} = q_p + q_n$ refers to the total amount of available Li-ions. It follows that $x_p + x_n = 1$. For Li-ion batteries, when fully charged, $x_p = 0.4$ and $x_n = 0.6$. When fully discharged, $x_p = 1$ and $x_n = 0$.

The different potentials are summarized in Fig. 1 (originally presented in (Daigle & Kulkarni, 2013)). The overall battery voltage $V(t)$ is the difference between the potential at the positive current collector, $\phi_s(0,t)$, and the negative current collector, $\phi_s(L,t)$, minus resistance losses at the current collectors (not shown in the diagram). At the positive current collector is the equilibrium potential $V_{U,p}$. This voltage is then reduced by $V_{s,p}$, due to the solid-phase ohmic resistance, and $V_{\eta,p}$, the surface overpotential. The electrolyte ohmic resistance then causes another drop V_e. At the negative electrode, there is a drop $V_{\eta,n}$ due to the surface overpotential, and a drop $V_{s,n}$ due to the solid-phase resistance. The voltage drops again due to the equilibrium potential at the negative current collector $V_{U,n}$. These voltages are described by the following set of equations:

$$V_{U,i} = U_o + \frac{RT}{nF}\ln\left(\frac{1-x_{s,i}}{x_{s,i}}\right) + V_{INT,i} \tag{14}$$

$$V_{INT,i} = \frac{1}{nF}\sum_{k=0}^{N_i} A_{i,k}\left((2x_{s,i}-1)^{k+1} - \frac{2x_{s,i}k(1-x_{s,i})}{(2x_{s,i}-1)^{1-k}}\right) \tag{15}$$

$$V_o = i_{app}R_o \tag{16}$$

$$V_{\eta,i} = \frac{RT}{F\alpha}arc\sinh\left(\frac{J_i}{2J_{i0}}\right) \tag{17}$$

$$J_i = \frac{i}{S_i} \tag{18}$$

$$J_{i,0} = k_i(1-x_{s,i})^{\alpha}(x_{s,i})^{1-\alpha} \tag{19}$$

$$V = V_{U,p} - V_{U,n} - V'_o - V'_{\eta,p} - V'_{\eta,n} \tag{20}$$

$$\dot{V}'_o = \frac{V_o - V'_o}{\tau_o} \tag{21}$$

$$\dot{V}'_{\eta,p} = \frac{V_{\eta,p} - V'_{\eta,p}}{\tau_{\eta,p}} \tag{22}$$

$$\dot{V}'_{\eta,n} = \frac{V_{\eta,n} - V'_{\eta,n}}{\tau_{\eta,n}} \tag{23}$$

Here, U_0 is a reference potential, R is the universal gas constant, T is the electrode temperature (in K), n is the number of electrons transferred in the reaction (n = 1 for Li-ion), F is Faraday's constant, J_i is the current density, and J_{i0} is the exchange current density, k_i is a lumped parameter of several constants including a rate coefficient, electrolyte concentration, and maximum ion concentration. $V_{INT,i}$ is the activity correction term (0 in the ideal condition). V_o is the voltage drops due to the solid-phase ohmic resistances, the electrolyte ohmic resistance, and the resistances at the current collectors. The τ parameters are empirical time constants (used since the voltages do not change instantaneously). This model contains as states $q_{s,p}$, $q_{b,p}$, $q_{b,n}$, $q_{s,n}$, V'_o, $V'_{\eta,p}$, and $V'_{\eta,n}$. The single model output is V .

By convention, the SOC of a battery is 1 when the battery is fully charged and 0 when the battery is fully discharged. In this model, it is analogous to the mole fraction x_n, but scaled from 0 to 1. The model distinguishes between nominal SOC and apparent SOC. Nominal SOC is computed based on the combination of the bulk and surface layer control volumes in the negative electrode, whereas apparent SOC is be computed based only on the surface layer. When a battery reaches the voltage cutoff, apparent SOC is 0, and nominal SOC is greater

than 0 (how much greater depends on the difference between the diffusion rate and the current drawn). Once the concentration gradient settles out, the surface layer will be partially replenished and apparent SOC will rise while nominal SOC remains the same. Nominal (SOC_n) and apparent (SOC_a) SOC are given by

$$SOC_n = \frac{q_n}{q^{max_n}}, \tag{24}$$

$$SOC_a = \frac{q_{s,n}}{q^{max_{s,n}}}, \tag{25}$$

where $q^{max_n} = 0.6q^{max}$ and $q^{max_{s,n}} = q^{max_n}\frac{v_{s,n}}{v_n}$.

Since the output voltage is a function of the mole fraction and the SOC is analogous to the mole fraction x_n (but scaled from 0 to 1), it can be said that the output voltage is actually a function of the SOC.

In order to get a good fit with the measured equilibrium potential, the number of terms in the expansion of $V_{INT,p}$ used in (Daigle & Kulkarni, 2013) is Np = 12 and in the expansion of $V_{INT,n}$ is Nn = 0, which results in 14 terms for $V_{U,p}$ and 2 terms for $V_{U,n}$. The parameters $A_{i,k}$ are determined by a fitting between the measured equilibrium potential and the curve defined by $V_{U,p} - V_{U,n}$. The equilibrium potential can be obtained by discharging the battery at a very slow rate, such that a concentration gradient will not build up, temperature is steady, and voltage drops due to internal resistances and other overpotentials are negligible.

However, the large number of terms and the complexity of the Eq. 14 and Eq. 15 result in a significant computational cost, which is not suitable for constrained computing platforms. Therefore, inspired by the equivalent circuit battery model by (Sierra, Orchard, Goebel, & Kulkarni, 2018), this work proposes an empirical parametrization of the curve that describes the equilibrium potential ($V_{U,p} - V_{U,n}$) as

$$V_U = v_L + \lambda \cdot e^{\gamma \cdot (1-x_{s,p})} - \mu \cdot e^{-\beta\sqrt{(1-x_{s,p})}}, \tag{26}$$

where v_L, λ, γ and μ and β are parameters to be estimated based on data.

Hence, Eq. 20 that describes the output voltage is then redefined as

$$V = V_U - V'_o - V'_{\eta,p} - V'_{\eta,n}. \tag{27}$$

Fig. 2 shows V_U (Eq. 26) fitted to the measured equilibrium potential for a 3S 5100mAh Li-Po battery as a function of mole fraction. The identified parameters through the curve fitting are given in Table 1. As aforementioned, the equilibrium potential can be obtained by discharging the battery at a very slow rate. This discharge cycle data is used to identify the parameters through a curve fitting between the measured voltage and the output voltage given by the model. The estimated parameters represent those achieving a least-squares (local) error minimum, which is satisfactory for our purposes.

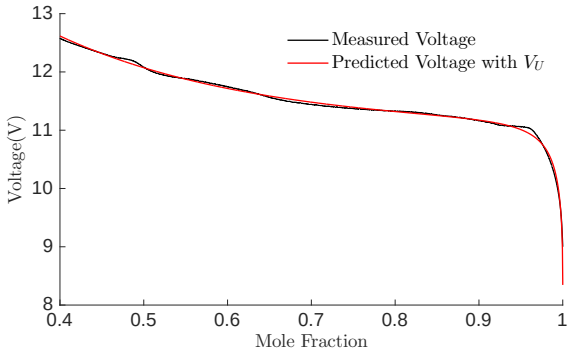

Figure 2. Measured and predicted open circuit potential.

Table 1. Equilibrium Potential Parameters for a 3S 5100mAh Li-Po Battery.

Parameter	Value
β	12.149
γ	4.240
λ	0.123
μ	2.822
v_L	11.044

Identified remaining model parameters are given in Table 2. Some parameters are defined by the battery dimensions and chemistry. The remaining parameters are estimated based on data, as with the parameters in Table 1.

Model validation for a variable loading scenario is shown in Fig. 3. Fig. 3b shows that the voltage predictions are reasonably accurate in response to changes in load. Some errors are still present that might be attributed to the fact the temperature effects are not included in the model.

3. APPLICATION TO PROGNOSTICS

SOC estimation and EOD prediction were performed to evaluate the effectiveness and efficiency of the proposed hybrid model. A Particle Filter (PF) with 100 particles is used as estimation algorithm and a Monte Carlo (MC) sampling-based algorithm with 100 samples is used to propagate the particles until reaching the failure threshold, that is, a voltage threshold V_{EOD}. We do not account for any uncertainty except for that provided in the state estimate, as our focus is on determining how accurate the model can predict EOD given precise information about the future and how efficient the model is concerning the original Electrochemistry-based model.

The discharges cycle data used in this study (originally presented in (Sierra et al., 2018)) correspond to delivery missions performed by a 3DR IRIS+ quadcopter shown in Fig.

Table 2. Remaining Battery Model Parameters for a 3S 5100mAh Li-Po Battery.

Parameter	Value
q^{max}	33660 C
R	8.3144621 J/mol/K
T	297 K
F	96487 C/mol
n	1
D	$6.8676 \cdot 10^{6}$ mol s/C/m^3
τ_o	1.026 s
α	0.5
R_o	0.018 Ω
S_p	$2.471 \cdot 10^{-4}$ m^2
k_p	$7.175 \cdot 10^{3}$ A/m^2
$v_{s,p}$	$1.031 \cdot 10^{-6}$ m^3
$v_{b,p}$	$1.747 \cdot 10^{-5}$ m^3
$\tau_{\eta,p}$	26.216 s
S_n	$5.207 \cdot 10^{-4}$ m^2
k_n	$5.716 \cdot 10^{4}$ A/m^2
$v_{s,n}$	$1.031 \cdot 10^{-6}$ m^3
$v_{b,n}$	$1.747 \cdot 10^{-5}$ m^3
$\tau_{\eta,n}$	15.967 s

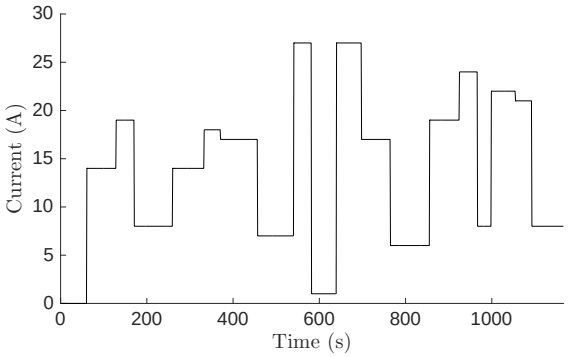

(a) Current

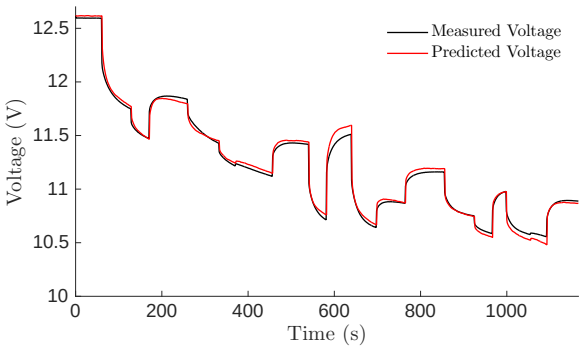

(b) Measured and predicted variable loading discharge curves.

Figure 3. Model validation for variable loading.

Figure 4. Multi-rotor platform used for validation. 3DR IRIS+ Quadcopter.

Table 3. Flight Plan No. 1.

No.	Maneuver	Payload (kg)	Translational speed (m/s)	Duration (s)
1	Take off & Climb (to 120 m)	0.3	1.5	80
2	Horizontal flight	0.3	6.0	210
3	Descent & land	0.3	0.5	240
4	Delivering payload	0.3	0.0	60
5	Take off & Climb (to 120 m)	0.0	1.5	80
6	Horizontal flight	0.0	6.0	210
7	Descent & land	0.0	0.5	240
8	Fully deplete battery	–	–	Until reaching the voltage threshold

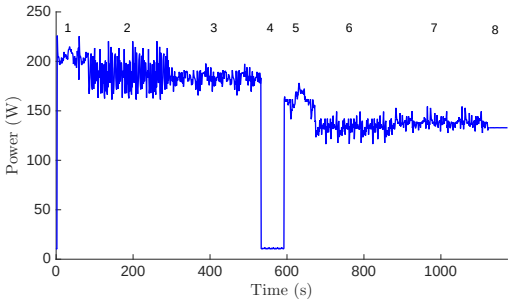

Figure 5. Power profile for flight plan No 1.

4 (from (3DR, 2013)) that uses a 3S 5100mAh Li-Po battery. Two flight plans are utilized for the analysis developed in this Section which are described in Table 3 and Table 4. Phase 8 in each flight corresponds to the discharge of the battery at the average of the power measured during phase 6. This discharge is made in order to safely obtain an approximate measurement for the amount of flight time that would have been supported by the battery if the multicopter had continued flying at approximately the same speed as it was going in phase 6. This measurement allows to compare battery EOD predictions made at various points over the mission, with the EOD time observed experimentally. For a voltage threshold (V_{EOD}) equal to 10.3 volts, the observed EOD time is 1274 seconds for the flight plan No. 1 and 1173 seconds for the flight plan No. 2.

To evaluate the effectiveness of the proposed hybrid model in prognostic, the following metrics are used in this analysis:

- EOD expectations, which is the instant k when the expectation of the battery voltage reaches the threshold:

Table 4. Flight Plan No. 2.

No.	Maneuver	Payload (kg)	Translational speed (m/s)	Duration (s)
1	Take off & Climb (to 120 m)	0.3	2.5	48
2	Horizontal flight	0.3	12.0	360
3	Descent & land	0.3	1.5	80
4	Delivering payload	–	0.0	60
5	Take off & Climb (to 120 m)	0.0	2.5	48
6	Horizontal flight	0.0	12.0	360
7	Descent & land	0.0	1.5	80
8	Fully deplete battery	–	–	Until reaching the voltage threshold

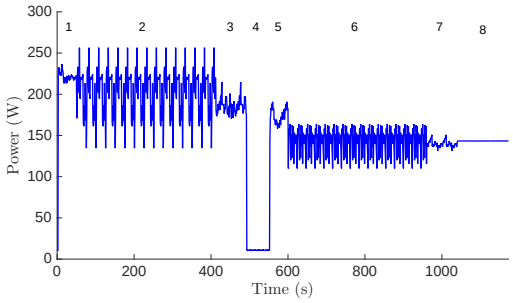

Figure 6. Power profile for flight plan No 2.

$$\widehat{EOD} \triangleq E\{k|E\{V(k)\} = V_{EOD}\}, \quad (28)$$

- The Just-In-Time Point ($JITP_{\gamma\%}$) value which specifies the cycle of operation where the probability of failure reaches a specified threshold γ (Engel, Gilmartin, Bongort, & Hess, 2000):

$$JITP_{\gamma\%} = \arg\min_{eod}(Pr\{EOD \leq eod\} \geq \gamma\%), \quad (29)$$

- The $\alpha - \lambda$ performance with the β criterion (Saxena et al., 2008; Saxena, Celaya, Saha, Saha, & Goebel, 2009):

$$\pi[r(k)]|_{\alpha^-}^{\alpha^+} = \sum_{\alpha^-}^{\alpha^+} \phi(x), \quad (30)$$

where $r(k)$ is the probability distribution of the predicted Remaining Useful Life (RUL) at time index k, ϕ is the non-parameterized probability distribution, and π is the total probability mass within $[\alpha^-, \alpha^+]$, being $\alpha^- = RUL^*(1-\alpha)$, $\alpha^+ = RUL^*(1+\alpha)$ and RUL^* the ground truth RUL. RUL distribution satisfies β criterion when $\pi[r(k)]|_{\alpha^-}^{\alpha^+} \geq \beta$.

The Prognostics Model Library (Daigle, 2016b) and the Prognostics Algorithm Library (Daigle, 2016a) by NASA Ames Research Center were used for the development of this study. MATLAB R2015b running on a Intel Core i5-2467QM CPU @ 1.60Ghz with 6GB of RAM was used to measure the processing times, making sure no other application was running at the same time.

Prognostic results for flight plan No. 1 and 2 using the hybrid model (assuming the future inputs are known) are shown in Fig. 7 and Fig. 9 correspondingly, and the average results of 50 realizations in terms of the above metrics are summarized in Table 5 and Table 6. Prognostic results for flight plan No. 1 and 2 using the electrochemistry-based model (assuming the future inputs are known) are shown in Fig. 8 and Fig. 10 correspondingly, and the average results of 50 realizations in terms of the above metrics are summarized in Table 5 and Table 6. The "True/False" labels in the $\alpha - \lambda$ performance figures denote if the β criterion is satisfied and the $5 - 25\%$ and $75 - 95\%$ bars correspond to ranges of the probability distribution of the predicted RUL.

Results tend to slightly overestimate the EOD as reported by (Daigle & Kulkarni, 2013) for variable loading discharges. This is more evident for flight plan No. 2 because its power profile is more variable. Nevertheless, results are within the desired $\alpha - \lambda$ performance. It should be mentioned that the variability of flight plan No. 2 is due to that the particular quadcopter used in this study tends to be more unstable when it carries its maximum payload at its maximum speed (presumably due to the configuration of its control system) which causes power peaks during horizontal flight.

Using the hybrid model, the maximum error for flight plan No. 1 in expected EOD time value is 21 seconds, that occurs when the prediction horizon is 315 seconds. For flight plan No. 2, the maximum error in expected EOD time value is 21 seconds when the prediction horizon is 264 seconds. Considering the length of the long-term prediction window, the maximum error between the ground truth and the expected EOD correspond to 6.66% and 7.95% respectively. Regarding Just-In-Time Point estimates, the values obtained for the $JITP_{5\%}$ are always smaller than the ground truth EOD, which provides a safe utilization of the asset when this metric is used to make decisions about the flight. In terms of the $\alpha - \lambda$ performance, the average of the probability mass, π, is 91.01% for flight plan No. 1 and 87.77% for flight plan No. 2.

Using the electrochemistry-based model, the maximum error for flight plan No. 1 in expected EOD time value is 34 seconds, that occurs when the prediction horizon is 315 seconds. For flight plan No. 2, the maximum error in expected EOD time value is 35 seconds when the prediction horizon is 264 seconds. Considering the length of the long-term prediction window, the maximum error between the ground truth and the expected EOD correspond to 10.79% and 13.25% respectively. Regarding Just-In-Time Point estimates, the values obtained for the $JITP_{5\%}$ are not always smaller than the ground truth EOD, which does not provide a safe utilization of the asset because the actual EOD might be before the end of the mission. In terms of the $\alpha - \lambda$ performance, the average of the probability mass, π, is 79.81% for flight plan No. 1 and 75.37% for flight plan No. 2.

Prediction results for both models are shown to be very accurate, but on average, the hybrid model performs slightly

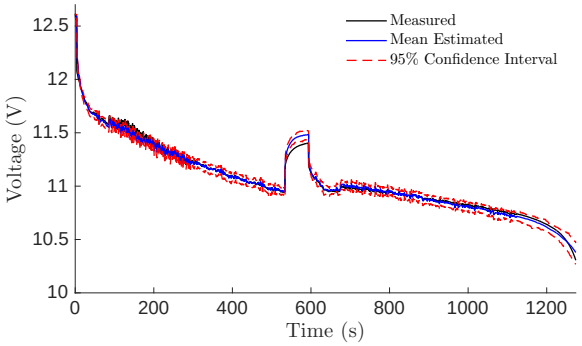

(a) Estimated Voltage

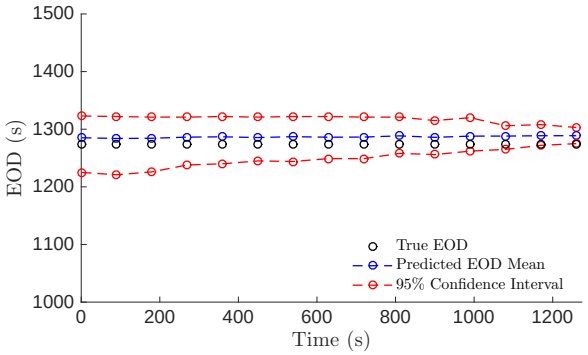

(b) Predicted EOD

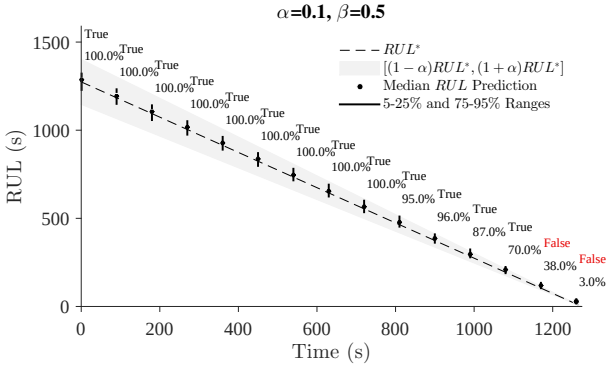

(c) $\alpha - \lambda$ performance

Figure 7. Prognostics results for flight plan No. 1 using the hybrid model.

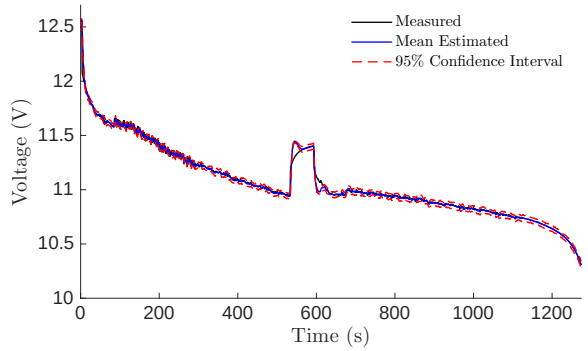

(a) Estimated Voltage

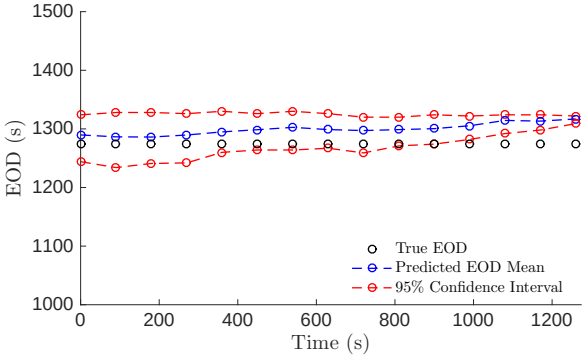

(b) Predicted EOD

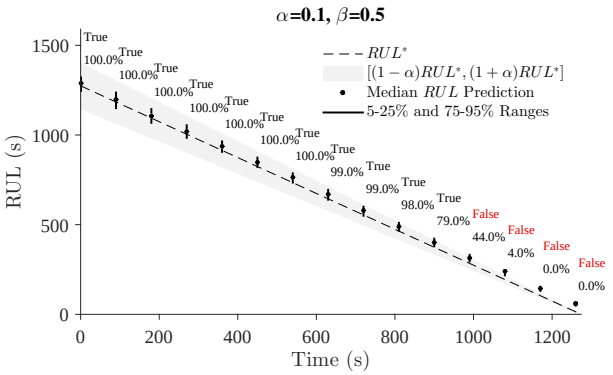

(c) $\alpha - \lambda$ performance

Figure 8. Prognostics results for flight plan No. 1 using the electrochemistry-based model.

Table 5. Average prediction results of 50 realizations for flight plan No. 1. True EOD at 1274 s

	Hybrid Model			Electrochemistry-based Model		
SOC	$\widehat{EOD}$	$JITP_{5\%}$	$\pi[r(k)]\|_{\alpha^-}^{\alpha^+}$	$\widehat{EOD}$	$JITP_{5\%}$	$\pi[r(k)]\|_{\alpha^-}^{\alpha^+}$
75% ($t = 267$ s)	1294 s	1247 s	100.00%	1292	1246	100.00%
50% ($t = 598$ s)	1295 s	1254 s	100.00%	1296	1257	99.88%
25% ($t = 959$ s)	1295 s	1266 s	73.02%	1308	1282	39.56%

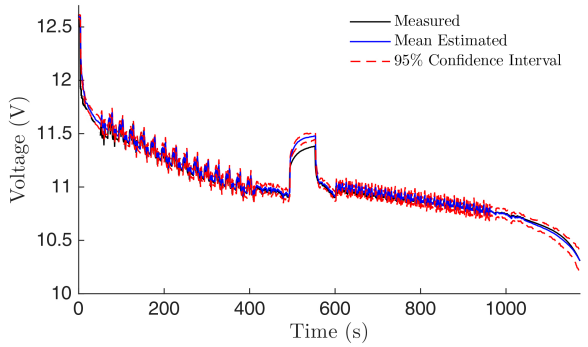

(a) Estimated Voltage

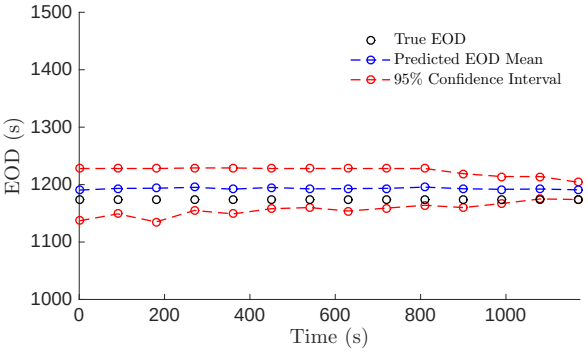

(b) Predicted EOD

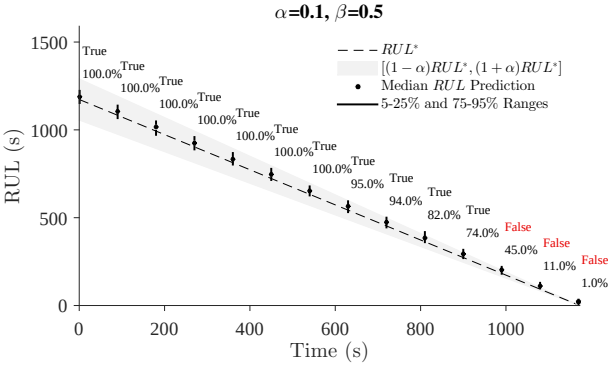

(c) $\alpha - \lambda$ performance

Figure 9. Prognostics results for flight plan No. 2 using the hybrid model.

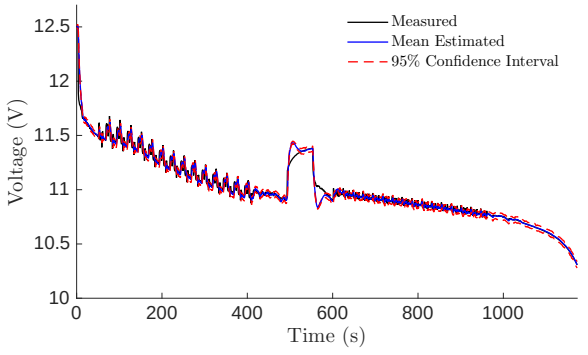

(a) Estimated Voltage

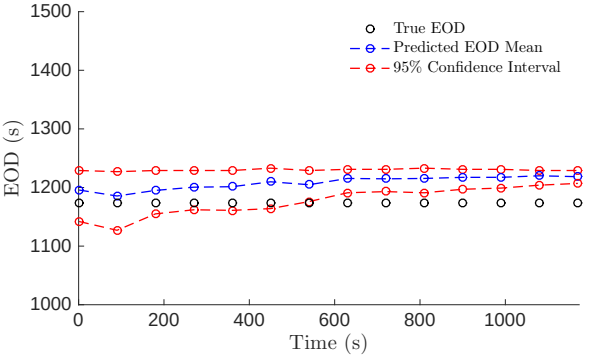

(b) Predicted EOD

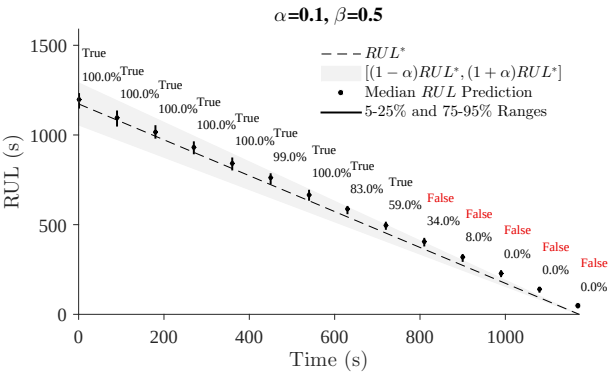

(c) $\alpha - \lambda$ performance

Figure 10. Prognostics results for flight plan No. 2 using the electrochemistry-based model.

Table 6. Average prediction results of 50 realizations for flight plan No. 2. True EOD at 1173 s

	Hybrid Model			Electrochemistry-based Model		
SOC	$\widehat{EOD}$	$JITP_{5\%}$	$\pi[r(k)]\|_{\alpha^-}^{\alpha^+}$	$\widehat{EOD}$	$JITP_{5\%}$	$\pi[r(k)]\|_{\alpha^-}^{\alpha^+}$
75% ($t = 248$ s)	1194 s	1150 s	100.00%	1195	1154	100.00%
50% ($t = 563$ s)	1193 s	1157 s	100.00%	1198	1165	99.48%
25% ($t = 909$ s)	1194 s	1167 s	66.32%	1208	1185	26.64%

better than the electrochemistry model. From the above analysis and as can be seen from Table 5, in terms of the average $\alpha - \lambda$ performance for flight plan No.1, the hybrid model is 11.2% more accurate than the electrochemistry-based model. Similarly, as can be seen from Table 6, in terms of the average $\alpha - \lambda$ performance for flight plan No.2, the hybrid model is 12.4% more accurate than the electrochemistry-based model. This improvement might be associated with the difficulty to find a good set of parameters that meet the constraints imposed by the model when the number of parameters is high. In particular, the proposed hybrid model requires off-line estimation of only 19 parameters, in contrast to the electrochemistry-based model that requires 30 parameters to be estimated off-line. In addition, the average estimation processing time per iteration (i.e. per time step) was measured for the proposed hybrid model and the electrochemistry-based model, using Unscented Kalman Filter (UKF) and Particle Filter (PF) as estimation algorithms. Table 7 and Fig. 11 present the results.

The average estimation processing time per iteration using the hybrid model is 69% of the time per iteration using the electrochemistry-based model when UKF is used as estimation algorithm, and it is 37% of the time per iteration using the electrochemistry-based model when PF with 100 particles is used as estimation algorithm. Also note that for the hybrid model, the estimation processing time when PF is used is lower than when UKF is used. Since PF has shown more accurate estimation results than UKF (Walker et al., 2015), the use of PF without increasing the processing times constitutes an advantage when one deals with constrained computing platforms such as that might be encountered on small UAVs.

Prediction processing time for a time window prediction of 1274 seconds using MC sampling-based prediction algorithm was also measured for different number of samples. The results are summarized in Table 8 and Fig. 12.

Prediction processing times are also shown considerably lower when the hybrid model is used, particularly when the number of samples increases. Prediction processing times with 10^2 and 10^5 samples using the hybrid model is 36% and 14%, respectively, of the prediction processing time using the electrochemistry-based model. This is attributed to the fact that Eq. 14 and Eq. 15 are computationally more complex than Eq. 26. Eq. 14 and Eq. 15 contain several summations and complex mathematical operations that require higher computational resources, while Eq. 26 that was proposed here to replace Eq. 14 and Eq. 15, is significantly less intense.

4. CONCLUSIONS

Considering the constrained processing power which may be encountered on small UAVs, in this paper, a hybrid battery model for battery prognostics is presented, which simplifies an electrochemistry-based battery model by substituting the electrochemistry characterization of the equilibrium potential by an empirical parameterization. The hybrid model was validated and applied to the prognosis of the EOD time of a Li-Po battery of a small quadcopter that performs delivery missions.

Table 7. Average estimation processing time per iteration.

Algorithm	Hybrid Model	Electrochemistry-based Model
UKF	$4.128e-3$ s	$5.905e-3$ s
PF ($N = 100$)	$2.425e-3$ s	$6.576e-3$ s

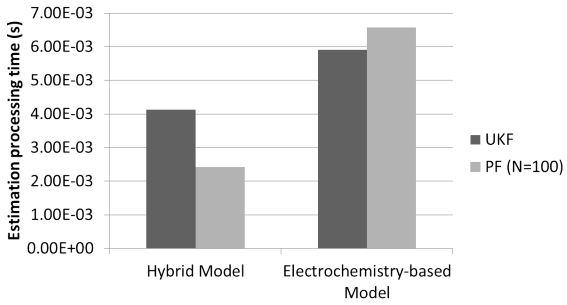

Figure 11. Estimation processing time per iteration.

Table 8. MC average processing time for a time windows of 1274 seconds.

Samples	Hybrid Model	Electrochemistry-based Model
10	2.088 s	3.376 s
50	2.820 s	5.438 s
100	3.182 s	8.853 s
500	3.608 s	24.778 s
1000	6.103 s	77.942 s
5000	17.321 s	114.981 s
10000	34.414 s	270.493 s
50000	115.197 s	1002.464 s
100000	267.997 s	1959.886 s

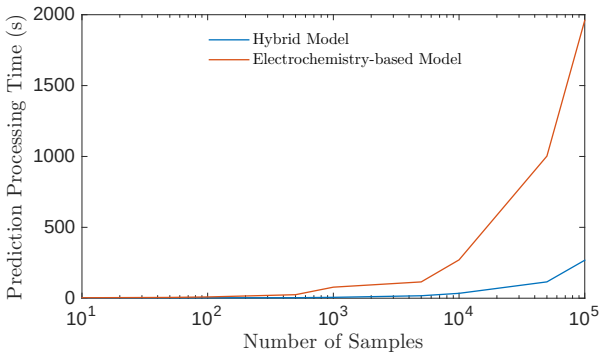

Figure 12. MC processing time for a time windows of 1274 second.

Prediction results were evaluated and compared with results obtained when the electrochemistry-based battery model is used. Both models perform very well, but on average, the hybrid model shows to perform slightly better than the electrochemistry model. Estimation and prediction processing times were also shown to be significantly lower than those obtained when the electrochemistry-based battery model is used. That is, the model described herein provides an effective and efficient approach for battery prognostics. Future work should include temperature effects on the discharge of the battery and describe how age-related parameters change over time. Temperature effects during discharge also should be tackled with an efficient approach for constrained computing platforms.

ACKNOWLEDGMENT

This work was supported in part by CONICYT under scholarship CONICYT-PCHA/Doctorado Nacional/2014-63140178, and in part by FONDECYT Chile Grant No. 1170044, the Advanced Center for Electrical and Electronic Engineering, AC3E, Basal Project FB0008, CONICYT. Also, the authors want to thank project CONICYT PIA ACT1405

REFERENCES

3DR. (2013). *Announcing iris, a totally ready-to-fly uav quadcopter with our next-gen autopilot.* https://3dr.com/blog/announcing-iris-a-totally-ready-to-fly-uav-quadcopter-with-our-next-gen-autopilot-53ac9d20558d/.

Banerjee, A., & Roychoudhury, A. (2017). Future of mobile software for smartphones and drones: Energy and performance. In *2017 ieee/acm 4th international conference on mobile software engineering and systems (mobilesoft)* (p. 1-12). doi: 10.1109/MOBILESoft.2017.1

Bole, B., Daigle, M., & Gorospe, G. (2014). Online prediction of battery discharge and estimation of parasitic loads for an electric aircraft. In *Annual conference of the prognostics and health management society 2014.*

Cuong, Q., Bole, B., Hogge, E., Vazquez, S., Daigle, M., Celaya, J., ... Goebel, K. (2013). Battery charge depletion prediction on an electric aircraft. In *Annual conference of the prognostics and health management society 2013.*

Daigle, M. (2016a). *Prognostics algorithm library [computer software].* https://github.com/nasa/PrognosticsAlgorithmLibrary.

Daigle, M. (2016b). *Prognostics model library [computer software].* https://github.com/nasa/PrognosticsModelLibrary.

Daigle, M., & Goebel, K. (2013). Model-based prognostics with concurrent damage progression processes. *IEEE Transactions on Systems, Man, and Cybernetics: Systems*, *43*(3), 535-546. doi: 10.1109/TSMCA.2012.2207109

Daigle, M., & Kulkarni, C. (2013). Electrochemistry-based battery modeling for prognostics. In *2013 international conference on prognostics and health management.*

de Souza Candido, A., Kawakami Harrop Galvao, R., & Yoneyama, T. (2014). Control and energy management for quadrotor. In *Control (control), 2014 ukacc international conference on* (pp. 343–348). doi: 10.1109/CONTROL.2014.6915164

Engel, S. J., Gilmartin, B. J., Bongort, K., & Hess, A. (2000). Prognostics, the real issues involved with predicting life remaining. In *2000 ieee aerospace conference. proceedings (cat. no.00th8484)* (Vol. 6, p. 457-469 vol.6). doi: 10.1109/AERO.2000.877920

Hogge, E. F., Bole, B. M., Vazquez, S. L., Celaya, J. R., Strom, T. H., Hill, B. L., ... Quach, C. C. (2015). Verification of a remaining flying time prediction system for small electric aircraft. In *Annual conference of the prognostics and health management society 2013.*

Mikolajczak, C., Kahn, M., White, K., & Long, R. T. (2011). *Lithium-ion batteries hazard and use assessment* (Tech. Rep.). The Fire Protection Research Foundation.

Pola, D., Navarrete, H., Orchard, M., Rabie, R., Cerda, M., Olivares, B., ... Perez, A. (2015). Particle-filtering-based discharge time prognosis for lithium-ion batteries with a statistical characterization of use profiles. *Reliability, IEEE Transactions on*, *64*(2), 710–720. doi: 10.1109/TR.2014.2385069

Saha, B., Quach, C., & Goebel, K. (2012). Optimizing battery life for electric UAVs using a bayesian framework. In *Aerospace conference, 2012 ieee* (pp. 1–7). doi: 10.1109/AERO.2012.6187365

Saha, B., Quach, P., & Goebel, K. (2011). Exploring the model design space for battery health management. In *Proceedings of the annual conference of the prognostics and health management society.* Montreal, Canada.

Saxena, A., Celaya, J., Balaban, E., Goebel, K., Saha, B., Saha, S., & Schwabacher, M. (2008). Metrics for evaluating performance of prognostic techniques. In *2008 international conference on prognostics and health management* (p. 1-17). doi: 10.1109/PHM.2008.4711436

Saxena, A., Celaya, J., Saha, B., Saha, S., & Goebel, K. (2009). On applying the prognostic performance metrics. In *2009 international conference on prognostics and health management.*

Sierra, G., Orchard, M., Goebel, K., & Kulkarni, C. (2018). Battery health management for small-size rotary-wing electric unmanned aerial vehicles: An efficient approach for constrained computing platforms. *Reliability Engineering & System Safety*. doi: https://doi.org/10.1016/j.ress.2018.04.030

Valavanis, K. P., & Vachtsevanos, G. J. (Eds.). (2015). *Handbook of unmanned aerial vehicles* (1st ed.). Springer Netherlands.

Walker, E., Rayman, S., & White, R. E. (2015). Comparison of a particle filter and other state estimation methods for prognostics of lithium-ion batteries. *Journal of Power Sources*, *287*, 1 – 12. doi: http://dx.doi.org/10.1016/j.jpowsour.2015.04.020

BIOGRAPHIES

M.Sc. Gina Sierra received the B.Sc. degree in Electronic Engineering (2008) and Master of Science in Information and Communicatiosn Technology (2013) from Universidad Distrital Francisco Jose de Caldas, Bogotá, Colombia. Currently, she is a doctoral candidate in Electrical Engineering at the University of Chile. She has worked in the areas of Artificial Intelligence and Machine Learning with application in diverse domains and topics such as electric aircraft, telecommunications networks, and control systems. Her current research interests include physics-based modeling and model-based diagnosis and prognosis.

Dr. Marcos E. Orchard is Associate Professor with the Department of Electrical Engineering at Universidad de Chile and was part of the Intelligent Control Systems Laboratory at The Georgia Institute of Technology. His current research interest is the design, implementation and testing of real-time frameworks for fault diagnosis and failure prognosis, with applications to battery management systems, mining industry, and finance. His fields of expertise include statistical process monitoring, parametric/non-parametric modeling, and system identification. His research work at the Georgia Institute of Technology was the foundation of novel real-time fault diagnosis and failure prognosis approaches based on particle filtering algorithms. He received his Ph.D. and M.S. degrees from The Georgia Institute of Technology, Atlanta, GA, in 2005 and 2007, respectively. He received his B.S. degree (1999) and a Civil Industrial Engineering degree with Electrical Major (2001) from Catholic University of Chile. Dr. Orchard has published more than 50 papers in his areas of expertise.

Dr. Chetan S. Kulkarni received the B.E. (Bachelor of Engineering) degree in Electronics and Electrical Engineering from University of Pune, India in 2002 and the M.S. and Ph.D. degrees in Electrical Engineering from Vanderbilt University, Nashville, TN, in 2009 and 2013, respectively. Since Jan 2013 he has been a Research Engineer II with SGT Inc. at the Prognostics Center of Excellence, NASA Ames Research Center. His current research interests include physics-based modeling, model-based diagnosis and prognosis focused towards electrical and electronic devices and systems. Dr. Kulkarni is a member of the Prognostics and Health Management (PHM) Society, AIAA and the IEEE.

Dr. Kai Goebel works at NASA Ames Research Center where he is the Area Lead for Discovery and Systems Health. He received the degree of Diplom-Ingenieur from Technische Universitaet Muenchen in 1990 and the Ph.D. from the University of California at Berkeley in 1996. Dr. Goebel worked at General Electrics Corporate Research Center in upstate New York where he was also an adjunct professor at Rensselear Polytechniq Institute. He has been on the dissertation committee of seven Ph.D. students at RPI, Syracuse University, University of Cincinnati, Vanderbilt University, Georgia Institute of Technology and Stanford University. He is currently guest professor at University of Cincinnati. He holds eighteen patents and he has published more than 300 technical papers.